Materials Science and Engineering C 30 (2010) 465–471

Contents lists available at ScienceDirect

Materials Science and Engineering C

journal homepage: www.elsevier.com/locate/msec

Thermal oxidation of vanadium-free Ti alloys: An X-ray photoelectron spectroscopy study

María Francisca López [a,*], Alejandro Gutiérrez [b], José Antonio Jiménez [c], Maria Martinesi [d], Maria Stio [d], Cristina Treves [d]

[a] Department of Surfaces and Coatings, ICMM-CSIC, Sor Juana Inés de la Cruz, 3, Cantoblanco, 28049 Madrid, Spain
[b] Departamento de Física Aplicada and Instituto Nicolás Cabrera, Universidad Autónoma de Madrid, Cantoblanco, E-28049 Madrid, Spain
[c] Centro Nacional de Investigaciones Metalúrgicas, CSIC, Avda. Gregorio del Amo 8, E-28040 Madrid, Spain
[d] Department of Biochemical Sciences of the University of Florence, Viale Morgagni 50, 50134 Florence, Italy

ARTICLE INFO

Article history:
Received 7 October 2009
Received in revised form 16 December 2009
Accepted 5 January 2010
Available online 13 January 2010

Keywords:
Titanium alloys
Biocompatibility
Oxidation
X-ray photoelectron spectroscopy (XPS)
Blood mononuclear cells

ABSTRACT

In the present work, X-ray photoelectron spectroscopy (XPS) was used to study the surface chemical composition of three alloys for biomedical applications: Ti–7Nb–6Al, Ti–13Nb–13Zr and Ti–15Zr–4Nb. The surface of these alloys was modified by annealing in air at 750 °C for different times with the aim of developing an oxide thick layer on top. The evolution of surface composition with annealing time was studied by XPS, and compared with the composition of the native oxide layer present on the samples before annealing. Two different oxidation trends were observed depending on the alloying elements and their corresponding diffusion kinetics, which give rise to different chemical species at the topmost layers. These results were linked with an evaluation of the biological response of the alloys by bringing them in contact with human peripheral blood mononuclear cells (PBMC).

© 2010 Elsevier B.V. All rights reserved.

1. Introduction

In the last years, biocompatible alloys have been studied and developed paying special attention to their corrosion behaviour, surface properties and biocompatibility. Among them, Ti–6Al–4V alloy exhibits excellent mechanical properties combined with optimal corrosion behaviour. However, there was much discussion about the toxic effect of V released in the body from this biomaterial [1–3]. Thus, a great effort is being devoted to the study of vanadium-free titanium alloys and their evaluation for surgical implant applications [4–6].

Physicochemical and electrochemical properties of an alloy and its long-term stability in biological environments play a decisive role for the biocompatibility. Corrosion of metallic biomaterials produces ion release, increasing their cytotoxicity. In the case of Ti alloys, the spontaneous formation of a surface oxide film protects the material from the physiological fluids and is the responsible of high corrosion resistance and biocompatibility [7–10]. Since the corrosion process and the affinity between bones and insert metals are closely related to the properties of the surface, different surface modification techniques have been applied on Ti alloys with the aim of improving as much as possible this property and to produce bioactivity. A possible way of achieving these goals is to increase the thickness of the protecting oxide layer. A classical, natural and cost-effective procedure used for growing thicker surface oxide layers is to heat the material in an oxygen rich atmosphere [11].

Taking into account the interest of investigating vanadium-free Ti alloys, in previous works three Ti alloys without V, Ti–7Nb–6Al, Ti–13Nb–13Zr and Ti–15Zr–4Nb, were evaluated as potential biomaterials [12]. Several properties of interest were studied, such as corrosion behaviour, surface topography, and microstructure. With the aim of enhancing their protection properties against corrosion attack, a simple thermal treatment in air at 750 °C for different oxidation times was applied, and the relevant properties were determined [13–16]. The chemical composition of the oxide layer is very related to the corrosion resistance. Consequently, several spectroscopic techniques were used to provide information on the components of the outer film. With this aim, Rutherford backscattering spectroscopy (RBS) and X-ray absorption spectroscopy (XAS) were used to estimate the in-depth chemical composition of the surface of the three alloys both before and after the oxide layers were grown [17,18]. However, since the last atomic layers of a biomaterial are directly in contact with biological tissues, the chemical determination of the topmost surface is really relevant. X-ray photoelectron spectroscopy (XPS) is a well-suited technique to perform surface analysis of materials, because it is rather surface-sensitive and provides information on the chemical composition of the last atomic layers (10–20 Å).

Cell culture systems for testing biological reactions to different agents, including biomaterials, have been gaining importance. A wide

* Corresponding author. Tel.: +34 91 334 9000; fax: +34 91 372 0623.
E-mail address: mflopez@icmm.csic.es (M.F. López).

0928-4931/$ – see front matter © 2010 Elsevier B.V. All rights reserved.
doi:10.1016/j.msec.2010.01.004

variety of cell lines are commonly used for biocompatibility tests: fibroblasts, epithelial and HeLa cells, keratinocytes, T lymphocytes from lymph nodes and macrophages obtained by lavage. Nevertheless, cytotoxicity tests *in vitro* will be more convincing when performed with cells that are homologous with the human tissue concerned, as pointed out by Wiegand and Hipler [19]. Therefore, considering that adverse inflammatory reactions may occur at the implant site, as a consequence of host–material interactions, and that acute inflammation and the foreign body response are induced by the inflammatory cell migration, many authors tested the biocompatibility of various biomaterials by culturing inflammatory cells, such as monocytes, lymphocytes, and macrophages. Seo et al. [20] suggested that the results of *in vitro* human peripheral blood mononuclear cell (PBMC) cultures, a heterogeneous cell population including monocytes and lymphocytes, may be considered closely related to the *in vivo* results of implantation. Human PBMC play a fundamental role in the response to inflammatory stimuli, which makes this system suitable for the study, *in vitro*, of the complex biological reactions resulting from cell–material interactions, and, consequently, to test the body response to biomaterials.

The mechanisms involved in the development of the inflammatory response are many, but a central role is played by the activation of leukocytes leading to the up-regulation of adhesion molecules on the cell surface. Thus, activation of cell adhesion molecules may be one of the consequences of the contact of biomaterials with host cells. Intercellular adhesion molecule-1 (ICAM-1) is an inducible transmembrane glycoprotein of the immunoglobulin family, which acting as a costimulatory molecule, is required for many inflammatory responses [21]. Therefore, those biomaterials inducing the lowest number of cells expressing ICAM-1 molecules are also expected to cause less short-term inflammation.

We report here the results obtained by XPS on the surface chemical composition of three V-free surface-modified titanium alloys developed for biomedical applications. Additionally, in order to verify the biocompatibility of the titanium alloys, these results were correlated with an *in vitro* biocompatibility study, which analyzed the levels of ICAM-1 protein produced when the different titanium samples were put in contact with human PBMC.

2. Materials and methods

2.1. Sample preparation

Three Ti basis alloys were prepared by arc melting and then casting in a copper coquille under high vacuum. The nominal composition of these alloys was (in wt.%) Ti–7Nb–6Al, Ti–13Nb–13Zr and Ti–15Zr–4Nb. A previous microstructural study revealed the existence of two different phases, α and β, forming a coarse microstructure with light and dark elongated grains [12]. In that work, the combination of scanning electron microscopy (SEM) and energy dispersive X-ray microanalysis (EDX) made possible the identification of both phases. Thus, the light region with a high level of Nb corresponds to β-phase while the dark region with negligible amount of Nb corresponds to α-phase. According to this result, it was confirmed that the ratio of α and β phases depends on the alloy composition. The oxidation treatment was performed on samples cut from as-cast ingots by electrospark erosion. Previous to the thermal treatment, the sample surfaces were abraded and polished using diamond paste with successively smaller particle size. Colloidal silica was used at the final step to ensure a surface free of mechanical deformation. Finally, the specimens were ultrasonically cleaned with acetone. At this stage, some samples were isothermally oxidized in air in a tube furnace at 750 °C for exposure times of 90 min, 6 h and 24 h. The different specimens were named as follows: Ti–7Nb–6Al as-received (T1-0), oxidized at 750 °C for 1.5 h (T1-1.5), 6 h (T1-6), and 24 h (T1-24); Ti–13Nb–13Zr as-received (T2-0), oxidized at 750 °C for 1.5 h (T2-1.5), 6 h (T2-6), and 24 h (T2-24); Ti–15Zr–4Nb as-received (T3-0), oxidized at 750 °C for 1.5 h (T3-1.5), 6 h (T3-6), and 24 h (T3-24).

2.2. X-ray photoemission spectroscopy

The composition of the oxide layer of the different materials was studied by X-ray photoemission spectroscopy (XPS). XPS spectra were recorded under ultra-high vacuum (UHV) conditions with a VG-CLAM hemispherical electron energy analyser using Mg X-rays as excitation source. The base pressure in the UHV-chamber during measurements was better than 10^{-9} mbar.

2.3. PBMC cultures

Before seeding with human PBMC cells, the samples, in as-received state or after the different heat treatments, were sterilized in an autoclave at 120 °C for 20 min. Human PBMC were obtained from healthy subjects by density gradient (1.077) centrifugation (30 min at 400 *g*) of heparinized venous blood diluted 1:2 with PBS (phosphate buffered saline) on Ficoll-Paque (research grade, Amersham Pharmacia Biotech). About 95% mononuclear cells at the interface, containing PBMC, was collected and washed twice with PBS. PBMC viability, checked by measuring Trypan blue dye exclusion, was >90%. PBMC were cultured in RPMI 1640 supplemented with 25 mM Hepes, 10% (v/v) heat inactivated FBS, 60 mg/ml (100 U/ml) penicillin, 100 mg/ml streptomycin, 0.29 g/l L-glutamine. Culture medium and all the other components were from SIGMA. PBMC were divided in 13 groups (2×10^6 cells/group): the cells of the control group received only culture medium; 12 groups were maintained in direct contact with the 12 sample types (one sample type for each group) for 48 h. Cultures were maintained at 37 °C in humidified atmosphere containing 5% CO_2. In all the experiments, when PBMC were collected, at the end of the incubation times, the adherent monocytes were scraped and added to the non-adherent cells. This method was selected over primary isolated monocytes, as it allowed to obtain quantities of cells sufficient for the programmed experiments.

2.4. Protein determination

Protein concentration in total cell lysates was determined by the Bradford method [22] using bovine serum albumin as standard.

2.5. Western blot analysis

At the end of the incubation periods, PBMC were collected and then lysed for 30 min at 4 °C in buffer containing 0.1% Nonidet P-40, 0.5% (wt/vol) sodium deoxycholic acid, 0.1% (wt/vol) SDS PBS, pH 7.4, and the following protease inhibitors: 0.5 mmol/l PMSF, 1 μg/ml leupeptin, 1 μg/ml aprotinin and 0.5 μg/ml pepstatin. All the products were from SIGMA. After centrifugation, the supernatant was used for protein determination and Western blot analysis. Electrophoresis was performed on 10% SDS-polyacrylamide gel, loading 10 μg protein per lane. Electrophoresed proteins were transferred onto pure nitrocellulose membranes (Bio-Rad Laboratories), as reported by Laemmli [23]. After transfer, the membranes were washed, incubated overnight at 4 °C with the antibody (Santa Cruz Biotechnology) to ICAM-1 (4 μg primary antibody/membrane), washed again, and then incubated for 60 min with the secondary horseradish peroxidase-linked antibody (Santa Cruz Biotechnology). The membranes, after two washes with TPBS, were treated with the chemiluminescent substrate and enhancer (ECL plus, Amersham). Blots were analyzed by Chemi-Doc (Bio-Rad), utilising the Quantity One program (Bio-Rad). Protein bands were normalized using the respective β-actin protein band. The data obtained by densitometric analysis are given relative to control (cells maintained in the culture medium alone), set equal to 100.

2.6. Statistical methods

Statistical significance was determined by either one-way ANOVA, followed by Bonferroni *t* test or by Student's *t* test. One-way analysis of variance was used to determine significance among groups, after which the modified *t* test with the Bonferroni correction was used for comparison between individual groups. Differences were considered significant at $P<0.05$.

3. Results and discussion

XPS spectra were recorded for the three Ti alloys before and after the heat treatment at 750 °C for different times. All spectra were analyzed by a least-squares fit in order to obtain information about the chemical states. The experimental data were described by using standard Gaussian–Lorentzian lines and the corresponding integral background. In all spectra, the solid line through the data points represents the result of the least-squares fit, with an additional dashed–dotted curve showing the integral background.

Fig. 1 shows the Ti-2p spectra of Ti–13Nb–13Zr for the as-received (T2-0) specimen as well as for the samples oxidized at 750 °C for the different treatment times (T2-1.5, T2-6 and T2-24). The three heat-treated Ti–13Nb–13Zr samples show similar XPS curves, with two peaks, which represent the doublet corresponding to the Ti 2p spin orbit splitting of the Ti^{4+} states. In these cases, the XPS emission indicates that the oxidation state of Ti in all heat-treated alloys is Ti^{4+}, being totally oxidized. The $2p_{3/2}$ emission of this Ti^{4+} component is located at a binding energy (BE) of ≈459.4 eV (dashed curve) and the $3p_{1/2}$ emission at ≈465 eV (dotted curve), with a spin orbit splitting of 5.6 eV. For the case of the as-received alloy, four doublets were needed to model the experimental XPS curve. These subspectra simulate the possible Ti oxidation states, i.e., Ti^{4+}, Ti^{3+}, Ti^{2+} and at lower binding energies Ti^{0}. This latter signal is ascribed to metallic Ti emission coming from the base material. The observation of a metallic signal in the as-received alloys can be explained because the thickness of the passive layer is approximately of the same order of magnitude as the XPS sampling depth. For Ti–15Zr–4Nb and Ti–7Nb–6Al the Ti-2p curves (not shown) have similar spectral shapes to those of the Ti–13Nb–13Zr samples. This result indicates that the three alloys have similar oxidation states at the surface, regarding Ti species. Thus, for the three Ti alloys, Ti is fully oxidized in the last atomic layers of the heat-treated specimens, whereas in the as-received samples the presence of several oxidation states in the passive layer was detected. The XPS data establish a fundamental difference between oxide layer

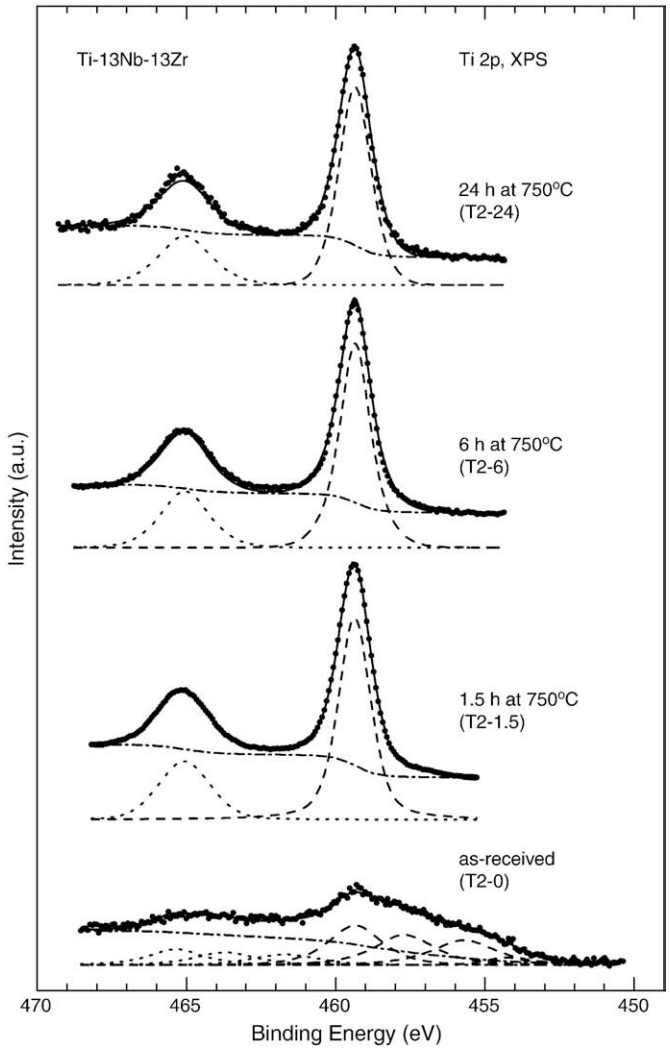

Fig. 1. Ti 2p spectra of Ti–13Nb–13Zr for as-received condition (T2-0) and oxidized at 750 °C for 1.5, 6 and 24 h (T2-1.5, T2-6 and T2-24, respectively). The solid line through the data points represents the results of a least-squares fit.

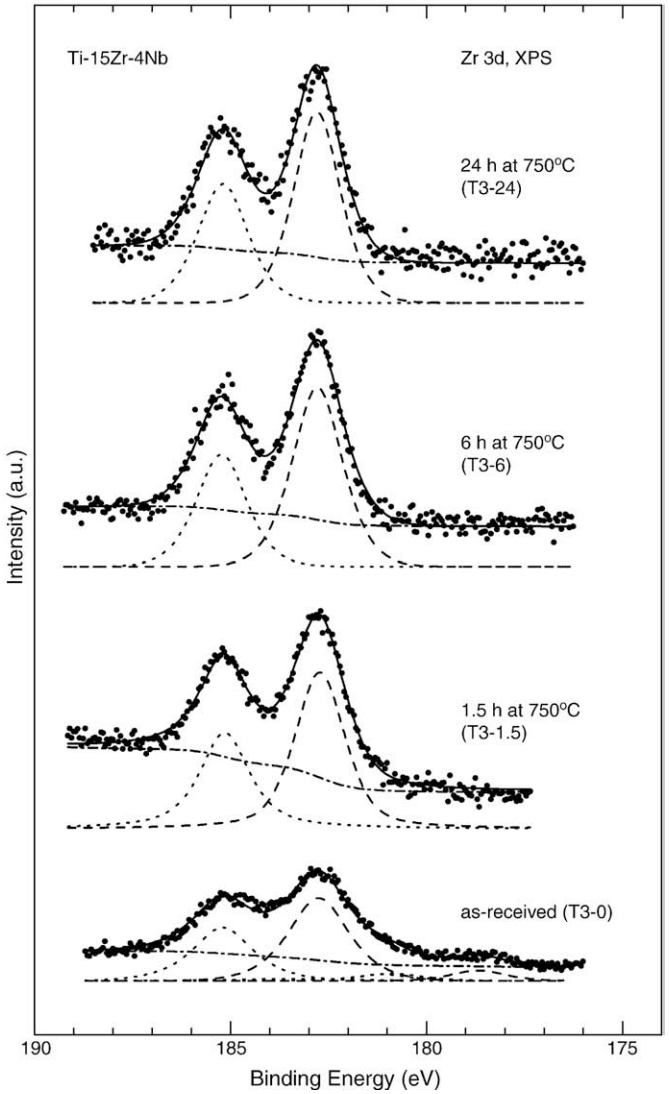

Fig. 2. Zr 3d spectra of Ti–15Zr–4Nb for as-received condition (T3-0) and oxidized at 750 °C for 1.5, 6 and 24 h (T3-1.5, T3-6 and T3-24, respectively). The solid line through the data points represents the results of a least-squares fit.

generated by heat treatment and native oxide layer grown spontaneously on the Ti alloy at room temperature.

The Zr-3d emission of Ti–15Zr–4Nb for the as-received (T3-0) and oxidized alloys (T3-1.5, T3-6 and T3-24) is shown in Fig. 2. A double structure is obtained for the case of the three oxidized Ti–13Nb–13Zr. These two peaks correspond to zirconium in the form of Zr^{4+}, separated by the spin orbit splitting, which is 2.4 eV. The $3d_{5/2}$ and $3d_{3/2}$ signals are located at binding energies of ≈182.7 eV (dashed curve) and ≈185.1 eV (dotted curve), respectively. The T3-0 sample shows an intense double structure together with a small contribution at lower binding energies. The first one, similar to that of the oxidized samples, is due to the fully oxidized Zr emission. The minor double structure located at binding energies ≈4 eV lower corresponds to Zr^0 (178.7 and 181.1 eV for $3d_{5/2}$ and $3d_{3/2}$ emissions, respectively). These peaks at lower binding energies can be ascribed to the metallic Zr signal coming from the base material. The Zr 3d XPS spectra of as-received and heat-treated Ti–13Nb–13Zr alloys are rather similar to those of Ti–15Zr–4Nb, suggesting for both materials an analogous behaviour. In both TiNbZr alloys, the as-received specimens exhibit a higher Zr^{4+} component with a small contribution of metallic Zr coming from the base alloy. For the heat-treated samples, the contribution of Zr in last atomic layers of the oxide film is in the form of Zr^{4+}, i.e., as fully oxidized chemical state.

Fig. 3 exhibits the Al 2p signal for all Ti–7Nb–6Al specimens, as-received and heat-treated. For the thermally oxidized samples as well as for the as-received sample, the presence of a single structure is observed. This emission located at a binding energy of ≈74.4 eV corresponds to fully oxidized Al.

For the Nb 3d XPS spectra of as-received and oxidized Ti–15Zr–4Nb alloys, the same fitting procedure was applied as can be observed in Fig. 4. In the case of the heat-treated alloys, the Lorentzian curves located at ≈207.5 eV BE correspond to the Nb $3d_{5/2}$ emission (dashed curve) and the subspectra located at ≈210.2 eV BE show the Nb $3d_{3/2}$ signal (dotted subspectrum). Both emissions clearly indicate that the chemical state of Nb in all thermally treated layers is Nb^{5+}. For the T3-0 sample more features have been observed at lower binding energies. The least-squares fit shows the doublet associated to Nb^{5+} and three additional double structures. These features correspond to the Nb $3d_{5/2}$ and $3d_{3/2}$ emission for lower oxidation states than Nb^{5+}: Nb^0, Nb^{2+} and Nb^{4+}. The Nb^0 contribution located at 202.8 eV and 205.5 eV comes from the alloy underneath the passive layer in metallic state. These results indicate the presence of different Nb oxide species in the passive layer. The XPS Nb 3d spectra for all Ti–13Nb–13Zr alloys show a similar behaviour to that of Ti–15Zr–4Nb suggesting an analogous tendency.

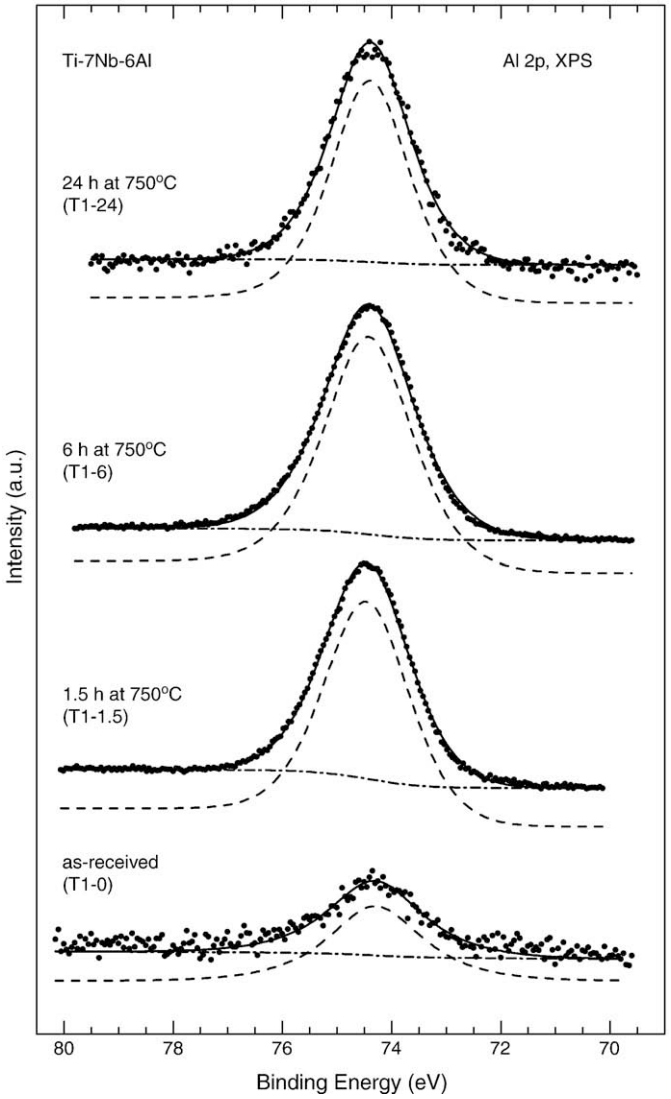

Fig. 3. Al 2p spectra of Ti–7Nb–6Al for as-received condition (T1-0) and oxidized at 750 °C for 1.5, 6 and 24 h (T1-1.5, T1-6 and T1-24, respectively). The solid line through the data points represents the results of a least-squares fit.

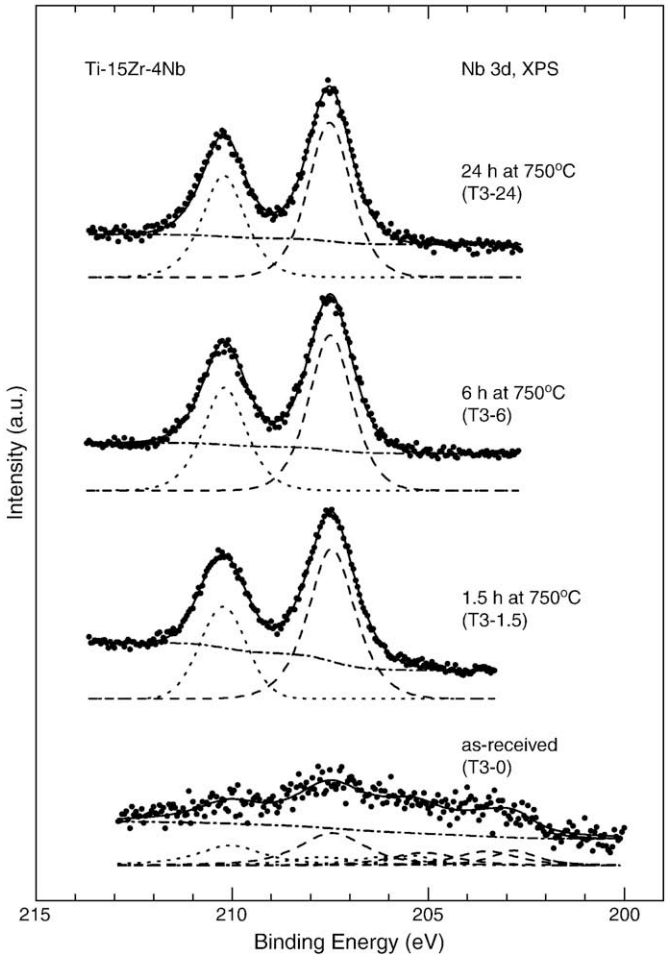

Fig. 4. Nb 3d spectra of Ti–15Zr–4Nb for as-received condition (T3-0) and oxidized at 750 °C for 1.5, 6 and 24 h (T3-1.5, T3-6 and T3-24, respectively). The solid line through the data points represents the results of a least-squares fit.

Table 1
Atomic percentages of the different alloying elements obtained from the XPS experiments at the surface of as-received Ti–7Nb–6Al, Ti–13Nb–13Zr and Ti–15Zr–4Nb (T1-0, T2-0 and T3-0) and after oxidation at 750 °C for 1.5, 6 and 24 h. For comparison, the corresponding bulk composition of the three alloys is also shown.

Ti alloys	Atomic percentages			
	Ti	Nb	Al	Zr
T1 bulk	85.9	3.6	10.5	–
T1-0	69.2	2.9	27.9	–
T1-1.5	25.5	0.0	74.5	–
T1-6	16.3	0.5	83.2	–
T1-24	12.8	0.0	87.2	–
T2 bulk	84.6	7.6	–	7.8
T2-0	55.9	5.1	–	39.0
T2-1.5	83.7	15.2	–	1.1
T2-6	78.0	19.7	–	2.3
T2-24	71.2	25.6	–	3.2
T3 bulk	89.1	2.3	–	8.6
T3-0	57.3	1.8	–	40.9
T3-1.5	92.4	5.8	–	1.8
T3-6	87.9	9.9	–	2.2
T3-24	80.1	14.6	–	5.3

Although it is important to identify the oxidation state of the different alloying elements both in the as-received and in the heat-treated alloys, the determination of the percentage of the different elements in the native or oxidized layer is also crucial. This information will reveal which are the main constituents and which are the minority species of the outer layers.

Table 1 exhibits, for the three Ti alloys, the atomic percentage values for the different oxidation states of all alloying elements considering as-received and oxidized specimens. For comparison, also the values corresponding to the bulk composition of the alloys are presented. Two different phenomena must be taken into account: the formation of a passive layer for the as-received samples and the generation of an oxide layer thermally favoured for the oxidized specimens. In the first case, on the surface of the alloys a spontaneous film is formed when the material is exposed to air. Although the initial element composition of the alloys corresponds to that of bulk material, diffusion processes give rise to a different composition at the surface. As it can be observed, the diffusion of Al from the bulk towards the surface is favoured for Ti–7Nb–6Al while Zr diffuses predominantly for the two TiNbZr alloys. For the three alloys, the formation of the passive layer at room temperature has a similar consequence: the decrease of the Ti contribution at the surface due to element diffusion of minority alloying elements from the bulk. In the case of the second phenomenon, i.e. the heat treatment of the alloys, different tendencies are observed. In the case of the TiNbAl alloy, the thermal process promotes the diffusion of Al towards the surface as in the non-thermal situation. However, for the two TiNbZr alloys at the initial stages of the heat treatment a large Ti diffusion is activated diminishing the surface Zr contribution observed for the passive layer. For longer times a slow decrease of the Ti contribution at the last atomic layers is produced due to the thermally activated Nb difussion from the bulk material.

Table 1 reveals the presence of an outer layer composed mainly of Al oxide with some Ti oxide contribution for Ti–7Nb–6Al, in contrast with the presence of Ti oxide with some contribution of Nb and Zr oxides for the two TiNbZr alloys. Previous studies performed with XAS (X-ray absorption spectroscopy) suggest for Ti–7Nb–6Al the formation of an outer Al_2TiO_5 layer at the first stages of the heat treatment [17]. As the oxidation times become longer an Al_2O_3 layer grows on the previous formed Al_2TiO_5 film. Although the sampling depth of XAS is around 70 Å, the more surface-sensitive XPS technique also points out to the substitution of Ti oxide by Al oxide at the last layers of the material upon oxidation. In this case, the Nb contribution is almost constant with the oxidation time. For the case of the two TiNbZr alloys, the XAS data revealed an outer layer composed mainly of TiO_2 for all oxidation times.

It is important to mention that surface characteristics are responsible for many properties of materials. In the case of biomaterials, one important attribute determined by the surface composition is the corrosion behaviour. In fact, the XPS results showed in Table 1 on the atomic surface composition support the conclusions of previous works [12,13] on the corrosion behaviour of the three Ti alloys without and with heat treatment as it will be explained below. Electrochemical techniques performed on the Ti alloys revealed that while upon oxidation Ti–7Nb–6Al improves its corrosion resistance, both TiNbZr alloys do not show any improvement of this property after heat treatment. The main parameter controlling this effect is the outer oxide layer. In the case of Ti–7Nb–6Al, the oxidation process generates an outer layer with a main contribution of Al_2O_3 but also with the presence of TiO_2. The film grown thermally for this alloy is thin, uniform and compact as it was determined by SEM [13]. An oxide layer with these characteristics protects the base material against corrosion. However, for the two TiNbZr alloys, the oxidation process generates an oxide layer with a main contribution of Ti oxide and the presence of Nb and Zr oxides. The resulting layer in this case is thick and porous showing some longitudinal fissures, as revealed previously by SEM [13]. A film with this morphology allows the penetration of the corrosive agents from the environment to the base material. Thus, as it was expected the surface composition of the three oxidized alloys has a direct influence on their corrosion behaviour. On the other hand, the corrosion behaviour will regulate the ion release, having an impact on the biocompatibility.

With the aim of relating the surface atomic composition with the biological response to inflammatory agents, the biocompatibility of Ti alloys in both as-received state and treated at 750 °C for 1.5, 6 and 24 h, was examined using human PBMC cultures. Thus, the protein levels of the adhesion molecule ICAM-1 in PBMC were determined after 48 h incubation by Western blot analysis. This incubation period may be considered a “short time”. However, the registration of early events in the interaction of PBMC with Ti alloys is highly relevant, bearing in mind that the inflammatory events at the early stages of implant integration and the dysregulation of inflammatory processes need to be carefully considered. In fact, the complexity of the host implant interface involves not only endothelial cells, but also circulating cells, which may react with endothelial cells to generate an inflammatory response.

In Table 2 the densitometric values for ICAM-1 protein levels registered after incubation of the PBMC with the sample types, and expressed as per cent of the values of control cells (PBMC maintained in the presence of culture medium alone), together with a representative Western blot, are reported. Although these data have been previously shown [24] they are here depicted, in order to better explain the correlation between the surface studies and a test of biocompatibility. As it can be observed in Table 2, with the exception of the samples T2-0 and T2-1.5, all the other sample types significantly increase ICAM-1 protein levels in comparison with untreated PBMC. T1-0 and T1-24 induce a similar increase in ICAM-1, but this increase is significantly lower if compared to that registered in the presence of T1-1.5 and T1-6. In the presence of T2-6 and T2-24, the increase in ICAM-1 protein levels is significant, the 24-h treatment significantly inducing higher levels if compared with the 6-h treatment. In the presence of the sample T3-6 the highest levels of ICAM-1 are detected, and, in the presence of T3-0, the lowest in comparison with the three heat-treated sample types, even if T3-0 induces a significant increase in comparison with untreated PBMC.

The ICAM-1 expression in PBMC shows in the Ti–7Nb–6Al case the best response for the fully oxidized specimen, while for the two TiNbZr alloys the lowest ICAM-1 values are exhibited by the untreated materials.

Table 2
ICAM-1 protein levels as determined by Western blot analysis in PBMC cultured for 48 h in the absence (PB, untreated PBMC) or in the presence of the as-received Ti–7Nb–6Al, Ti–13Nb–13Zr and Ti–15Zr–4Nb (T1-0, T2-0 and T3-0) and the alloys after oxidation at 750 °C for 1.5, 6 and 24 h. To detect possible differences in protein loading, the membrane was stripped and reprobed with anti-β-actin antibody. Protein bands were normalized using the respective β-actin protein band. Top, representative Western blot. Bottom, quantitative data. Blots were scanned by densitometry, and data, reported as a percentage of the control value (untreated PBMC), set equal to 100, are expressed as the mean ± SD of three separate experiments. $^{*}P<0.01$ (in comparison with untreated PBMC); $^{\circ}P<0.01$ (in comparison with T1-1.5 and T1-6); $^{\wedge}P<0.01$ (in comparison with T2-0, T2-1.5, and T2-24); $^{''}P<0.01$ (in comparison with T2-0, T2-1.5, and T2-6); $^{+}P<0.01$ (in comparison with the oxidized samples); $^{=}P<0.01$ (in comparison with T3-0, T3-1.5, and T3-24).

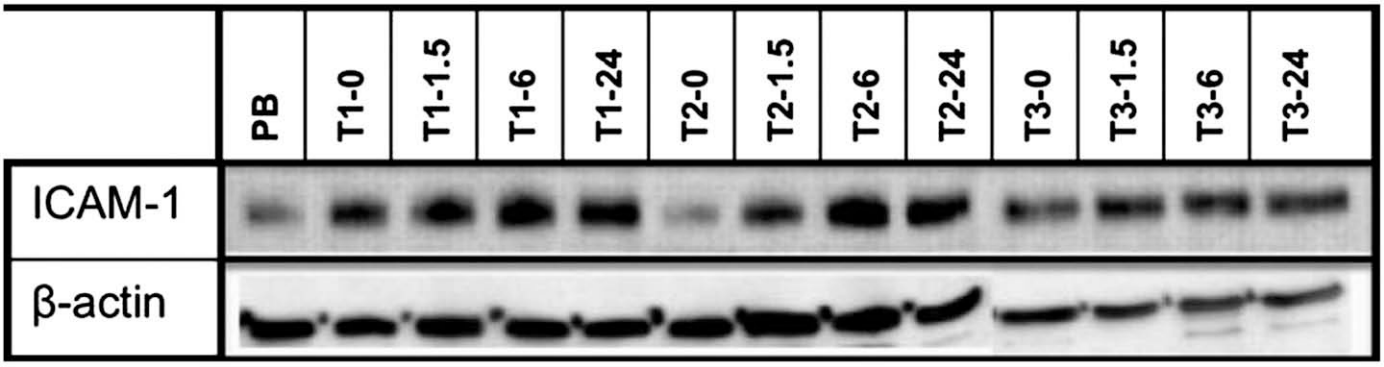

Sample state	ICAM-1 protein expression		
	Ti–7Nb–6Al (T1)	Ti–13Nb–13Zr (T2)	Ti–15Zr–4Nb (T3)
0	190.4 ± 6.6*°	106.0 ± 3.0	193.4 ± 6.0*+
1.5	279.3 ± 25.0*	121.0 ± 10.7	249.7 ± 18.5*
6	303.8 ± 5.0*	225.2 ± 12.6*^	337.1 ± 27.6*=
24	174.8 ± 13.8*°	279.6 ± 4.0*''	249.2 ± 7.0*

As deduced from these experiments, the Ti–7Nb–6Al alloy improves its biological response upon oxidation. In contrast, for the case of the two TiNbZr alloys, the best behaviour is exhibited by the samples without heat treatment. These results are in agreement with the surface atomic composition data and with previous corrosion experiments.

4. Conclusions

XPS experiments were performed to study the chemical composition of the last atomic layers of Ti–7Nb–6Al, Ti–13Nb–13Zr and Ti–15Zr–4Nb alloys in both, as-received state and after thermal treatments in air at 750 °C for different times. Two different oxidation behaviours were observed depending on the alloying elements:

a) XPS spectra of Ti–7Nb–6Al samples show Al enrichment on the surface oxide layer relative to the bulk composition. Al content in the outer layer increases from 28 at.% prior to oxidation to 75, 73 and 87% in the samples oxidized for 1.5, 6 and 24 h, respectively. Therefore, the formation of the surface oxide film is predominantly governed by Al diffusion. The resulting outer layer is compact, thin, uniform and composed mainly by Al_2O_3 with small amounts of TiO_2. Previous corrosion studies showed an improvement in the corrosion behaviour of these heat-treated samples.
b) XPS spectra of TiNbZr alloys show Zr enrichment on the surface oxide layer relative to the bulk composition only in as-received materials. However for the heat-treated alloys, Ti propagation towards the surface is favoured. The resulting oxide layer is composed mainly by Ti oxide, with some contribution of both Zr and Nb oxides, giving rise to a less protective layer.

To evaluate the biocompatibility of the alloys for the different conditions, the samples were put in contact with human peripheral blood mononuclear cells in culture, and the ICAM-1 adhesion molecule levels were determined. For the Ti–7Nb–6Al alloys, the best biological response was given by the fully oxidized sample. In contrast, for the two TiNbZr alloys, the data exhibit a better behaviour for the as-received specimens. These results are in agreement with previous corrosion studies where the oxidation process was shown to be beneficial only for the Ti–7Nb–6Al alloy. The surface chemical composition of the specimens, as determined by XPS, supports the biological results.

Acknowledgements

This work has been partially supported by the Spanish MEC under Projects MAT-2008-01497/NAN, MAT-2007-66719-C03-03, MAT-2006-13348 and CSD2007-00041, and by grants from Italian MIUR.

References

[1] S.G. Steinemann, in: G.D. Winter, J.L. Leray, K. De Groot (Eds.), Evaluation of Biomaterials, Wiley, New York, 1980.
[2] S.D. Rogers, D.W. Howie, S.E. Graves, M.J. Pearcy, D.R. Haynes, J. Bone Jt. Surg. 79 (1997) 311.
[3] Y. Okazaki, E. Nishimura, Mater. Trans., JIM 41 (2000) 1247.
[4] Y. Okazaki, S. Rao, Y. Ito, T. Tateishi, Biomaterials 19 (1998) 1197.
[5] K. Maehara, K. Doi, T. Matsushita, Y. Sasaki, Mater. Trans. 43 (2002) 2936.
[6] N.T.C. Oliveira, A.C. Guastaldi, Acta Biomater. 5 (2009) 399.
[7] J.E.G. Gonzalez, J.C. Mirza-Rosca, J. Electroanal. Chem. 471 (1999) 109.
[8] S. Tamilselvi, V. Raman, N. Rajendran, Electrochim. Acta 52 (2006) 839.
[9] J. Pan, D. Thierry, C. Leygraf, Electrochim. Acta 41 (1996) 1143.
[10] M. Könönen, M. Hormia, J. Kivilahti, J. Hautaniemi, I. Thesleff, J. Biomed. Mater. Res. 26 (1992) 1325.
[11] M.F. López, A. Gutiérrez, M.C. García-Alonso, M.L. Escudero, J. Mater. Res. 13 (1998) 3411.
[12] M.F. López, A. Gutiérrez, J.A. Jiménez, Electrochim. Acta 47 (2002) 1359.
[13] M.F. López, J.A. Jiménez, A. Gutiérrez, Electrochim. Acta 48 (2003) 1395.
[14] C. Munuera, T.R. Matzelle, N. Kruse, M.F. López, A. Gutiérrez, J.A. Jiménez, C. Ocal, Acta Biomater. 3 (2007) 113.
[15] A. Gutiérrez, C. Munuera, M.F. López, J.A. Jiménez, C. Morant, T. Matzelle, N. Kruse, C. Ocal, Surf. Sci. 600 (2006) 3780.
[16] D. Cáceres, C. Munuera, C. Ocal, J.A. Jiménez, A. Gutiérrez, M.F. López, Acta Biomater. 4 (2008) 1545.
[17] M.F. López, L. Soriano, F.J. Palomares, M. Sánchez-Agudo, G.G. Fuentes, A. Gutiérrez, J.A. Jiménez, Surf. Interface Anal. 33 (2002) 570.
[18] A. Gutiérrez, F. Pászti, A. Climent-Font, J.A. Jiménez, M.F. López, J. Mater. Res. 23 (2008) 2245.
[19] C. Wiegand, U.C. Hipler, Skin Pharmacol. Physiol. 22 (2009) 74.
[20] Y.K. Seo, H.H. Yoon, Y.S. Park, K.Y. Song, W.S. Lee, J.K. Park, Cell Biol. Toxicol. 25 (2009) 513.
[21] G. Hartmann, A.M. Krieg, Gene Ther. 6 (1999) 893.
[22] M.M. Bradford, Anal. Biochem. 72 (1976) 248.
[23] U.K. Laemmli, Nature 227 (1970) 680.
[24] C. Treves, M. Martinesi, M. Stio, A. Gutiérrez, J.A. Jiménez, M.F. López, J. Biomed. Mater. Res. A 92A (2010) 1623.